Available online at www.sciencedirect.com
SCIENCE DIRECT®
International Journal of Heat and Mass Transfer 49 (2006) 2610–2618
International Journal of HEAT and MASS TRANSFER
www.elsevier.com/locate/ijhmt

Adiabatic and diabatic measurements of the liquid film thickness during spray cooling with FC-72

A.G. Pautsch, T.A. Shedd *

Multiphase Flow Visualization and Analysis Laboratory, University of Wisconsin-Madison, 1500 Engineering Drive, Madison, WI 53706-1609, USA

Received 15 June 2005; received in revised form 9 January 2006
Available online 31 March 2006

Abstract

An experimental investigation was performed to measure the liquid film thickness created by both a low flow rate single nozzle and a high flow rate four-nozzle array spray design using FC-72. Measurements were made using a non-intrusive optical technique based on total internal reflection. Reflected light rings that formed on a test die were photographed, and an automated program measured and recorded the radii, from which the thickness of the film was calculated using fundamental equations of geometric optics. This measurement technique was used to investigate the dependence of the film thickness on location and applied power. For a four-nozzle array, regions of the die that have been previously shown to exhibit the poorest heat transfer performance were found to have the thickest films, in agreement with qualitative imaging. With the single-nozzle spray, it was found that adding a heat load did not affect the film thickness. Away from the spray impact region, the applied heat caused a significant amount of localized dryout.

Keywords: Spray cooling; Film thickness; Optical measurement

1. Introduction

As semiconductor technology progresses, the removal of the heat generated within the shrinking devices is becoming a difficult parameter to control. One example is the integrated circuit, where an increase in density and frequency translates to increasing power dissipation. The ideal thermal management system should provide high heat removal rates uniformly over a large area. Spray cooling is a very promising candidate to address the thermal concerns of systems requiring high heat flux removal in a compact volume. This is demonstrated by its successful commercial application in the Cray X1 vector supercomputers [1] and the numerous patents that have been granted for various spray cooling applications. Application to future generations of high heat flux devices, however, will require more uniform surface coverage and higher peak heat fluxes. The critical heat flux (CHF) of spray cooling with the use of Fluorinert liquids is 60–150 W/cm^2 at this time, depending on test conditions. The CHF sets the limits of the peak performance of spray cooling. In order to raise this limit, a better understanding of the physics associated with the spray cooling process must be gained. Possibly the most important – and one of the least studied – parameters of spray cooling is the thickness of the liquid film layer that exists on the heated surface.

Spray cooling is a complicated process in which a cooling fluid is delivered to a hot surface by a spray atomizer. In many electrical applications, this fluid is the fluorocarbon perfluorohexane, trade name FC-72 (®, 3M). The liquid flows into an atomization nozzle that breaks the flow into many droplets. These droplets hit the surface and are swept off by the flow of subsequent droplets. The surface is continually wetted in this manner, and a thin liquid film forms. In this film, heat transfer is related to a number of mechanisms, including conduction, convection,

* Corresponding author. Tel.: +1 608 2652930; fax: +1 608 2628464.
E-mail address: shedd@engr.wisc.edu (T.A. Shedd).

0017-9310/$ - see front matter © 2006 Elsevier Ltd. All rights reserved.
doi:10.1016/j.ijheatmasstransfer.2006.01.024

Nomenclature

n_1	refractive index of glass	θ	angle of refraction
n_2	refractive index of liquid	$\theta_{c,13}$	critical angle between the glass and liquid
n_3	refractive index of air	$\theta_{c,23}$	critical angle between the liquid and air
R	radius of light ring [m]	1	first medium
t_{film}	thickness of the liquid film [m]	2	second medium
t_{base}	thickness of the glass heater [m]		

nucleation, de-saturation of the gas, and bubbles entrained by impacting droplets. The contribution of each of these components to the total heat removal process is unknown, and all are related to the thickness of the film.

The objective of this study was to measure the liquid film thickness distribution beneath the single- and four-nozzle sprays in a production spray cooling system. To accomplish this, a non-intrusive optical film thickness measurement system was fabricated, as detailed below. Results were obtained for the film thickness distribution due to a four-cone spray array under adiabatic conditions and compared with visualization of the same spray array. The film thickness at locations beneath a single-cone spray with and without applied heat flux was also measured, and the results compare favorably with recent measurements performed by the authors and others.

2. Review of previous work

Previous experiments have attempted to measure the thickness of the thin film in spray cooling. The experiments were run using water as the test fluid with an air-atomizing nozzle [2]. An average value of the maximum thickness of the film was measured using Fresnel diffraction and the variation of the film thickness was measured using a holographic method. It was found that, with a constant air pressure, increasing the flow rate of the water led to an increase of the film thickness. The thickness of the film was found to be between 85 and 235 μm, depending on the flow rate of the water. Using the holographic method, these researchers concluded that the variation in the thickness of the film was less than 1 μm in the area of the film that was studied.

An earlier estimate of film thickness was made by Tilton by measuring the film thickness after the hydraulic jump of a single nozzle with a needle mounted on a traversing measuring scope [3]. Based on continuity requirements for a single-phase film, the film thickness was estimated before the hydraulic jump, in the area under the spray. Uncertainties of approximately 200 μm in the measurements of the film thickness after the hydraulic jump led to an estimated uncertainty of 10% in the values for the film thickness under the spray. It was assumed that the film had a uniform thickness under the spray. Film thickness values were reported at 120–350 μm. These measurements were taken adiabatically.

A variation of the method presented in this paper was used to determine the instantaneous thickness of a film resulting from the impingement of fuel spray on a flat, horizontal surface [4]. These researchers measured film thicknesses of 20–50 μm for films of iso-octane resulting from 110 to 350 μm droplets impinging at velocities of 10–21 m/s. Other numerical models have been developed to predict the film thickness in non-adiabatic conditions [5]. Assuming a constant volumetric flow rate, film thickness values between 1.0 and 1.8 μm were predicted for heat fluxes of 28.4–12.2 W/cm^2, respectively.

3. Experimental apparatus

3.1. Film thickness measurement

The purpose of this experiment was to determine the film characteristics for a prototype of the spray cooling system used in the Cray X1 multichip modules. The spray configuration is shown in Fig. 1; a spray plate, approximately 7 mm below the chip surfaces, contains a series of nozzles so that each integrated circuit is cooled according to its power dissipation. It is not possible to implement the film thickness measurement techniques described above due to this confined geometry. The non-intrusive optical technique used in this research involves the total internal reflection of light at an interface between materials with two different indices of refraction (n_1 and n_2). The theory of this method can be derived from Snell's Law, Eq. (1)

$$n_1 \sin(\theta_i) = n_2 \sin(\theta_t) \tag{1}$$

When n_1 is greater than n_2, an incident angle θ_i can be determined that will lead to the transmission angle θ_t being 90°. At this point, none of the light is transmitted and all that is not absorbed is reflected back at a reflectance angle $\theta_r = \theta_i$. The angle at which this occurs is the angle of total internal reflection, which is also called the critical angle.

When measuring the film thickness using the total internal reflection method, light must be scattered from a light source in all directions. This is accomplished using a light diffuser. When the scattered light hits an interface at incident angles less than the critical angle, most of the light intensity is transmitted and a small part is reflected. At the critical angle, all of the light is reflected. This light bounces back to the outer wall surface and hits the diffusing material, and a light ring forms around the source of

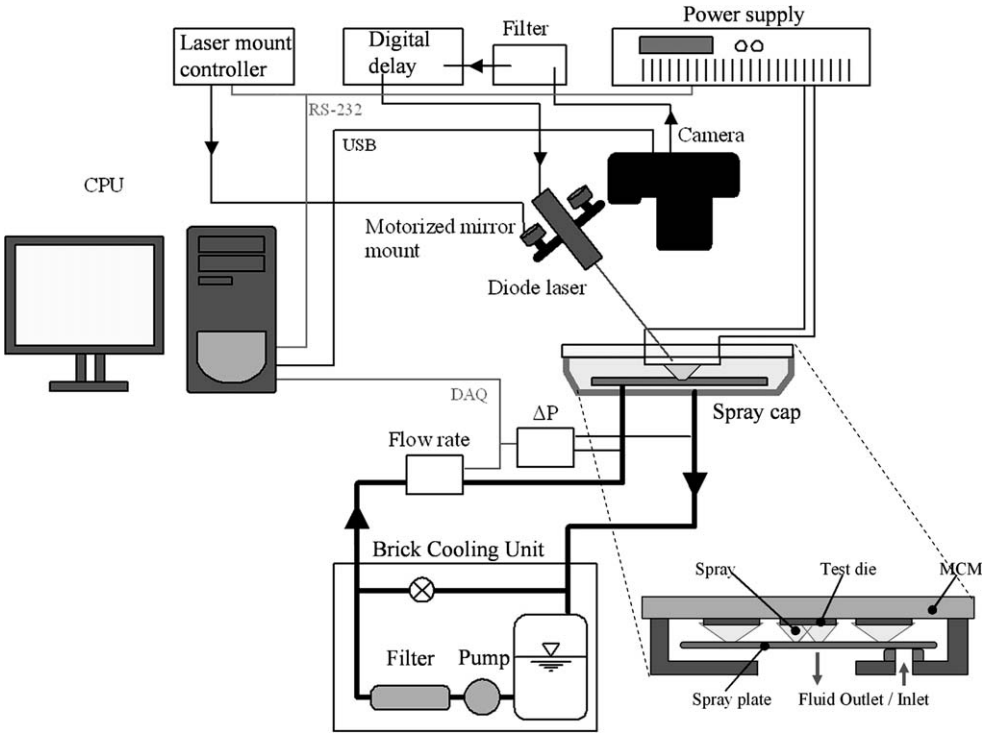

Fig. 1. Schematic of the film thickness test stand and spray cap.

light. A camera captures this, and the diameter of the resulting light ring is measured. The diameter of the light ring is proportional to the total distance that the light travels on its round trip through the wall and liquid. Thus, if the wall thickness is known, the thickness of the film can be determined once the radius of the light ring has been found [6,7]. It should be noted that if the liquid thickness is approximately 1.5 times the thickness of the transparent wall, the light will strike the solid/liquid interface at an angle greater than the critical angle for that interface and a constant light ring corresponding to the thickness of the wall will appear [6]. This is referred to as the "outer ring". The exact value of the limiting liquid thickness depends on the refractive index ratio between the liquid and the wall.

Although the theory of the measurement technique has been derived for an ideal liquid interface, the spray system generates a highly disturbed, wavy film. To determine whether or not this system was still valid in these cases, Rodríguez and Shedd [8] performed an in situ verification of the measurement using the turbulent thin film of annular two-phase flow. Using indexed-matched materials and a fluorescent dye in the liquid, cross-section images of the turbulent film were obtained and measured via image processing. This experiment found that the optical film thickness technique agreed very will with the mean film thickness measured using the fluorescent imaging. Further investigation found that the optical method functions only when a rather significant amount of averaging is performed. For example, the exposure time of the image needed to be at least 0.01 s in order to obtain an average reflected ring from the wavy surface. In addition, several images are averaged to obtain a final film thickness measurement. These averaging operations allow the system to obtain accurate mean film thickness measurements of wavy films.

In order to fully visualize the entire spray-affected surface, a transparent test die was developed for this experiment. The dies had a 2000 Å coating of indium tin oxide (ITO) on one side of a 17 mm × 17 mm × 0.5 mm piece of Corning 1737 aluminosilicate glass. Positive and negative lead wires were attached to the die using a silver-composite epoxy to create a transparent resistive heating element. To make film thickness measurements, the side of the die that did not have the ITO coating was made into a diffuse surface by applying a thin layer of paint. The dies were secured to a mounting surface using a clear UV-curing

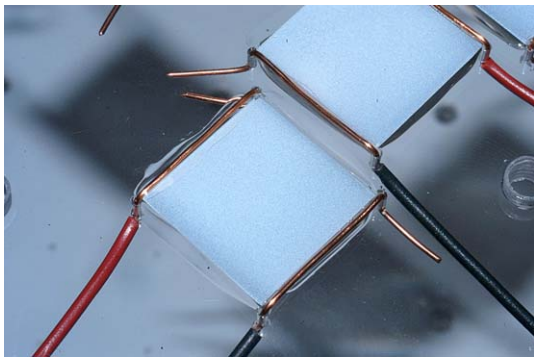

Fig. 2. The test dies implemented had a thin coating of metal sputtered on one face and a thin layer of paint applied to the other.

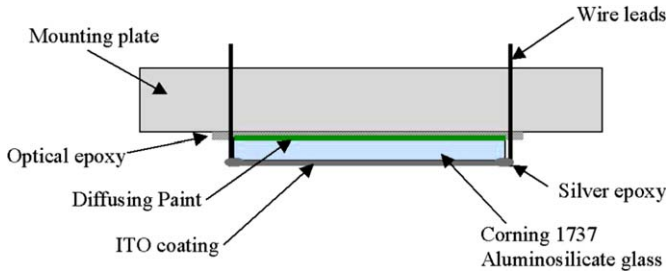

Fig. 3. Schematic of the mounted die.

optical epoxy. The epoxy also creates a seal so that fluid cannot seep under the dies and distort the image. This assembly is shown in Fig. 2, and a schematic is shown in Fig. 3. To power the dies, a Xantrex XDC 6 kW power supply was connected to the terminals of the dies. The unit could be controlled through the computer, and measures current to 5 mA and voltage to 10 mV. During operation, it was discovered that the combination of high liquid flow rates and high electrical current to the dies would cause both the silver epoxy on the electrical connections and the epoxy that held them onto the backer plate to erode. For this reason, images of the powered die were taken last and were taken in bursts of six images, such that the power supply would be on for as short of a time period as possible.

The complete test section consisted of four transparent die assemblies on a 4 mm thick polycarbonate mounting plate. The dies were cooled by spray nozzles that atomized the fluid and projected the spray upward (against gravity) onto the die surface. The spray nozzles were housed in a stainless steel spray plate that was mounted inside of a stainless steel spray cap. Each spray plate contained two different sets of spray nozzles, a single-nozzle and a four-nozzle array, as seen in Fig. 4. The atomizers used to produce the spray were pressure swirl atomizers with two inlet slots per nozzle orifice. Center jets were present to produce a full cone spray.

Images of the light rings were taken with a Nikon D100 6.1 MPixel digital SLR camera with a Tamron 55 mm macro lens. The shutter speed was set to 0.004 s, which corresponded to the fastest shutter speed that would capture the entire laser pulse. The aperture was set to its lowest setting, *f*4.5. The camera was mounted directly above and perpendicular to the test section. The flash output signal of the camera was filtered and fed into a digital delay generator (Berkeley Nucleonics Corp. Model 555-4), which would turn the laser on for 175 ms. The laser used as the source of light was a Lasiris 635 nm 3.5 mW diode laser that was designed to be modulated via an external pulse input. It also contained integrated focusing optics that were adjusted to obtain a small point of light on the test surface. A smaller light source gives a higher contrast in the light ring, making it easier to find the diameter of the ring related to the total internal reflectance.

3.2. Fluid delivery system

The fluid was delivered to the test section by a Brick Cooling Unit (BCU) produced by Cray Inc. The fluid delivery system was comprised of a fluid reservoir, pump, various filters, flow meter, system manifold, spray cap, and spray plate. A schematic of this facility is shown in Fig. 1. The pump was a custom designed gear pump manufactured by MicroPump. Considerations in material selections for pump parts were made based on the properties and solubility of the test fluid being used. The pump was magnetically coupled to a Leeson 1/2 horsepower AC motor. The fluid was run through a 5 μm particulate filter to remove any particles suspended in the fluid. After the particulate filter, a portion of the fluid was directed through a fluid conditioning by-pass loop to remove perfluoroisobutylene (PFIB), dissolved oxygen and water vapor. This fluid was returned to the reservoir after filtration. The fluid that did not pass through the filter by-pass loop passed through a flow meter. The flow meter was a NIST-traceable Model G112 McMillan turbine flow meter which was calibrated for use with the test fluid using a graduated cylinder and stopwatch. The manufacturer's calibration indicated an uncertainty for the flow measurements of less than 2% of reading. The total uncertainty including the test fluid calibration curve is a maximum of 5% of reading at the lowest flow rates.

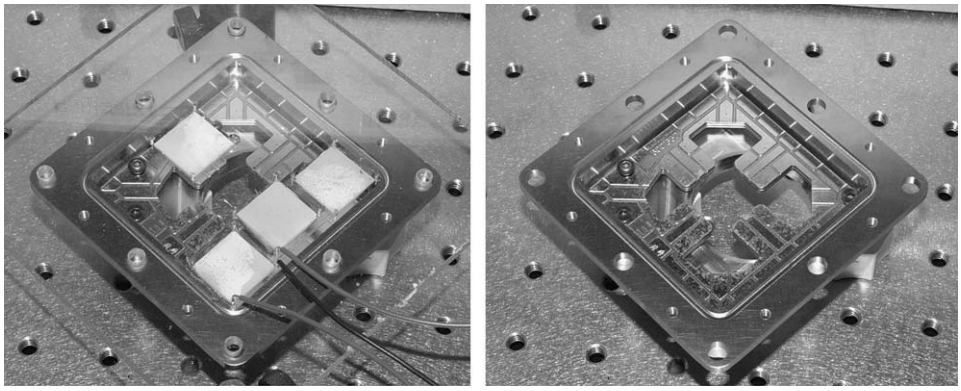

Fig. 4. The heater test plate on and off of the spray cap.

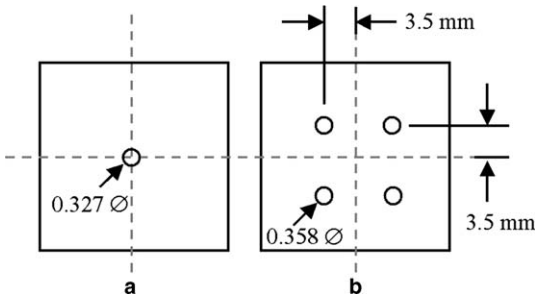

Fig. 5. Size and location of the spray nozzles relative to the die for (a) the single-nozzle and (b) the multi-nozzle array. All dimensions in mm.

The fluid then passed to the spray cap, which delivered the fluid to the test section by a spray plate orientated to deliver the fluid in an upwards direction such that the draining would be gravity assisted. The pressure difference across the spray cap was measured with a Setra 0–345 kPa differential pressure transducer, which has uncertainty of ±0.86 kPa. The signals from the flow meter and pressure transducer were reported to a PC through a data acquisition device, a National Instruments NI PCI-6023E 12-bit card with a CB-68LP break-out box. Fluid leaving the spray cap returned to the reservoir. The reservoir was a 5 liter stainless steel vessel.

Tests were performed with two different spray nozzle arrays. A nozzle array is defined as a nozzle or set of nozzles designated to cool one die. The nozzles were designed and manufactured by Parker Hannifin Corp. Each nozzle was a pressure swirl atomizer consisting of a swirl chamber, two inlet slots, and a center jet to form a full spray cone [7]. The orifices of the nozzles were 0.358 mm in the four-nozzle array and 0.327 mm in the single-nozzle array, as seen in Fig. 5. The centers of the nozzle arrays were located 6.8 mm directly below the centers of the test dies and the spray was directed upwards.

3.3. Data extraction

With the images acquired, measurements of the light ring radii were performed using the commercial program Matlab 7.0.1, with the Imaging Toolbox [9]. Each image was originally a 6.1 MPixel color image. A red diode laser was used, so the primary color in the images was red, but at the center of the image, the laser spot was bright enough to saturate the green and blue pixels as well. To find the location of the laser spot for each image, the green color plane was extracted. This image was thresholded, and a centroid was found. The location of the centroid was used as the center of the search area for the radii. Because of the large size of the 6.1 MPixel files, the program was slow to run using the full image. To shorten the time to analyze each image, it was cropped based on the location of the center of the laser to an approximately 1 MPixel image. This image was then filtered with a Gaussian filter and an averaging filter to remove as much noise as possible. To choose the radius search area of this smaller image, the limits were

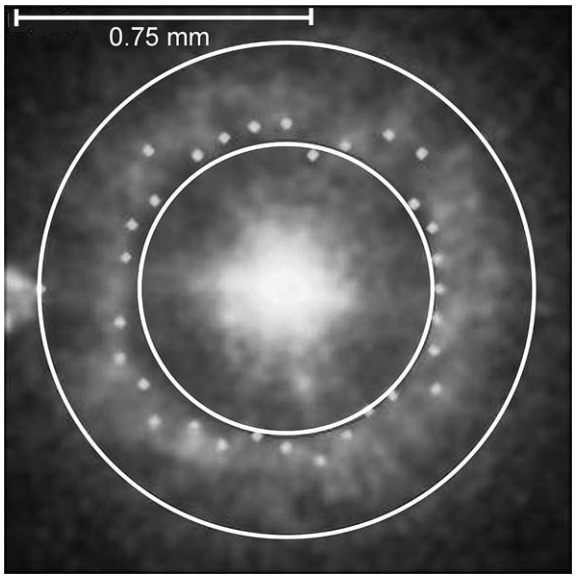

Fig. 6. Image of ring finding program showing the dry radius (inner light circle), flooded radius (outer light circle) and the radii measured (light dots).

estimated based on the two extreme radii that can exist: the dry radius and the flooded radius. These radii are drawn in Fig. 6 as the inner and outer circles. A padding of 10 pixels was then added to both ends of the search area to avoid numerical discontinuities near the edges.

A simple gradient kernel was convolved with the pixel intensities in the image to find the value of the radii: the location of the ring was defined as the point of largest intensity gradient. The subprogram that was written to find the radii locations searches in only four directions: top, bottom, left, and right. Instead of rotating the search directions in an image, the image is rotated and then fed back into the same subprogram. A bi-cubic interpolation was used to perform the image rotation. Each of the radii found was plotted as a dot, as seen in Fig. 6. The values of these radii were also recorded in an array. After all images were processed, a low-pass filter was applied to removed any radii larger than the flooded radius, or outside of the outer circle. These values are where no ring was found, and are not used in analysis. The array and the standard deviation of the remaining radii were calculated. The average value of the radii was used in another subprogram to calculate the film thickness, with known indices of refraction, glass thickness, and scaling factor. The subprogram is based on the principles of total internal reflection. With some simplification and substitution, the film thickness (t_{film}) can be found using Eqs. (2) and (3),

$$t_{\text{film}} = \frac{0.5R - t_{\text{base}} \tan(\theta_{c,13})}{\tan(\theta_{c,23})} \tag{2}$$

$$\theta_{c,23} = \sin^{-1}\left(\frac{n_3}{n_2}\right), \quad \theta_{c,13} = \sin^{-1}\left(\frac{n_3}{n_1}\right) \tag{3}$$

where R is the radius of the ring times the scaling factor, $\theta_{c,13}$ is the angle of total internal reflection between the

glass in the die and the air, and $\theta_{c,23}$ is the angle of total internal reflection between the fluid and the air.

At some locations on the die, there were very small cracks in the paint on the die that formed while the paint was drying. When these cracks are present, the ring finding program will choose the edge of the crack as the point of largest gradient and assume that it is the location of the ring. To eliminate these improper data points, another filter was used to further reduce the data from images in which cracks were present. For each search direction, the statistical mode (most frequent radius) was found. Every radii that was within one pixel of this mode was eliminated. This would remove all of the radii that were associated with cracks. It will also eliminate some valid radii, but enough will remain that a reliable average radius will be found.

Each individual image has a resolution of about 3.5 μm/pixel. However, a large number of images were obtained at each location. As noted by Shedd and Newell [10], the use of multiple samples improves the uncertainty of the mean, so the results are reported with sub-pixel precision. The uncertainty in the film thickness varies from location to location because of the fluctuating nature of the film, but it ranged from ±0.7 μm to ±0.5 μm.

4. Results and discussion

4.1. Film thickness distribution

The film thicknesses were measured for the four-nozzle array at each of the locations shown in Fig. 7. To generate a full-surface thickness profile that could be compared with the flow visualization, the film thickness values measured in the upper left quadrant were mirrored in the other three quadrants to fill in only the unmeasured locations. Then, film thickness values at intermediate nodes were interpolated as an average of their four nearest measured nodes (three for the edges). This generates the nearly symmetric surface map representing the mean film thickness distribution shown in Fig. 8. Although symmetry was artificially imposed by this algorithm, it is justified by the nearly symmetrical values measured at the marked locations in each of the four quadrants.

All of the data points were obtained for a combined flow rate of 3.65 mL/s (0.863 mL/s per nozzle). As the figure shows, there is a peak of maximum thickness in the center of the die. There are also thicker areas along the lines of horizontal and vertical symmetry. All of these areas correspond to areas of interaction between the different nozzles. Compare this with the instantaneous image of the film shown above the measured film thickness map, which shows that a thicker film builds up in the regions between the sprays. There are, apparently, instantaneous fluctuations in the flow rates from each nozzle, causing the cross-like interaction region to fluctuate in position. However, the qualitative agreement between the instantaneous visualization and the averaged optical film thickness measurements is quite good.

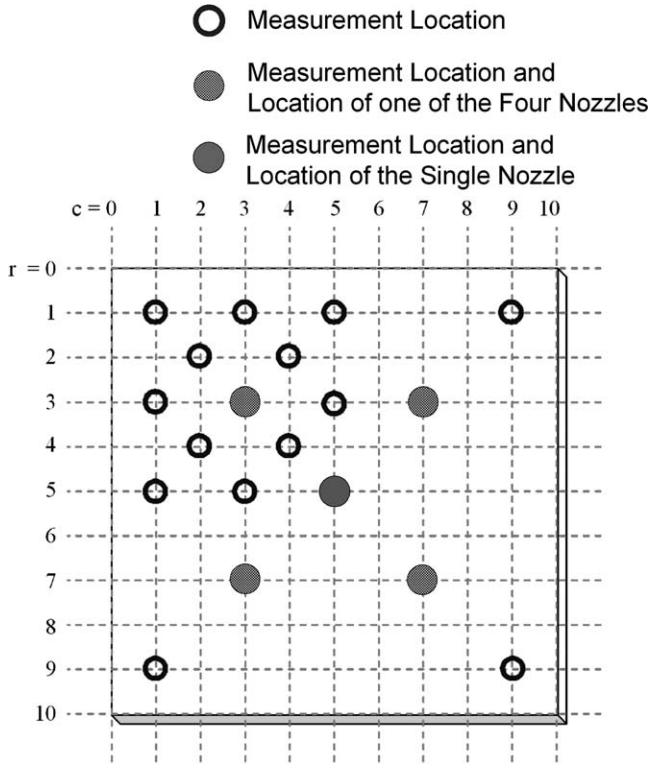

Fig. 7. Locations of film thickness measurements for four-nozzle array were based on a grid system (r, c). For the single nozzle, only locations (2,2) and (4,4) were analyzed.

Other experiments that measured heat transfer coefficients for the same nozzle design have found that the poorest performance occurs in the same regions that were found to have a thicker film [11]. Also, the point where critical heat flux first occurred was always at the center of the die, the location of the largest film thickness. This is not to say that the heat transfer performance is the poorest due to the film thickness, but it is likely that the flow behavior that caused the film to thicken in this area also caused the heat transfer coefficient to drop. For this particular design, the flow behavior causes stagnation between the nozzles in the areas where the flows interact.

4.2. Film thickness and applied heat flux

Due to the difficulty in obtaining large data sets for powered dies, a detailed surface map was not performed for the four-nozzle array with applied heat flux or for the single nozzle in either adiabatic or powered conditions. Instead, heat was applied to the die and the film thickness was measured with and without power at two locations, (2,2) and (4,4), which are specified in Fig. 7. Position (4,4) is located at the edge of the spray impact region where the droplet density was thinner and the transition to the film flow began for the single-nozzle spray. Position (2,2) is located in a purely film flow region. The results from this experiment are shown in Table 1. The table shows that film thickness measurements were obtained for only one flow rate,

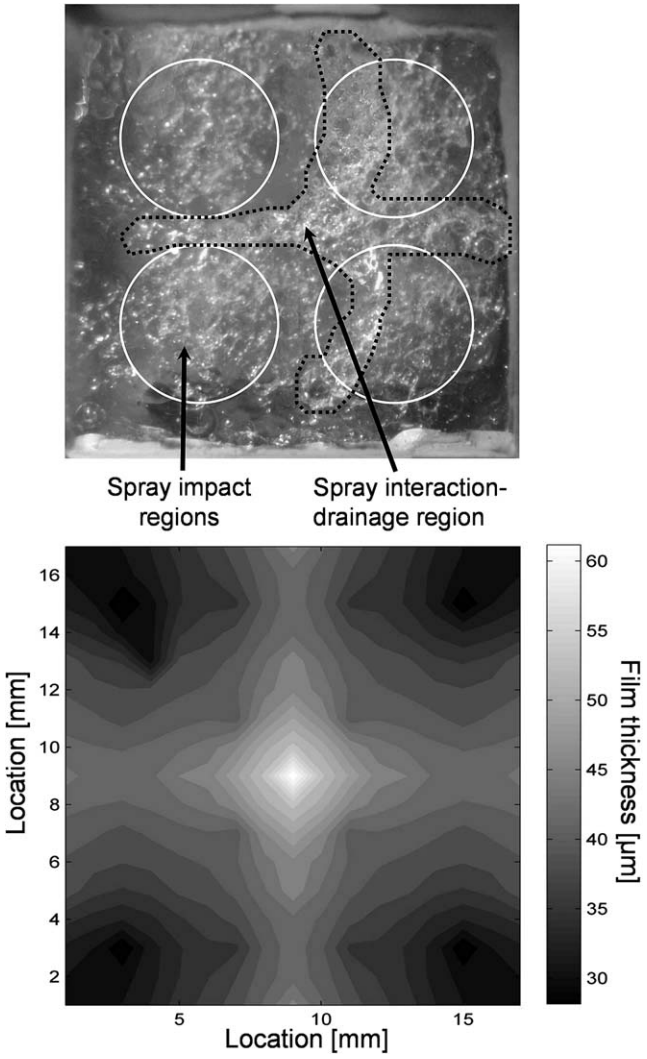

Fig. 8. Photograph of instantaneous liquid film distribution and the contour plot of film thickness measured on four-nozzle array.

0.863 mL/s, which corresponded to a pressure of 200 kPa across the nozzles. The entries in the table with the flow rate set to 0 mL/s show the results of measurements of the light ring for a the dry surface for comparison.

A heat flux of either 0 or 15 W/cm^2 was applied. The critical heat flux for this nozzle design at this flow rate was previously measured to be 23 W/cm^2, and the operating point for this test was chosen to be approximately 2/3 of this value to avoid letting the die getting too hot [11]. The liquid temperature liquid temperature was kept very near to room temperature, or $T_{liq} = 26$ °C; since the liquid was gas-saturated FC-72 at 1 atm, this corresponded to a gas-subcooled condition with $T_{sat} = 56$ °C. It was not possible to measure the wall temperature with the current apparatus. Similar flow conditions on a thermal test vehicle generated an average die temperature of approximately $T_{wall} = 66$ °C [11].

Reviewing the results, the film thickness at the edge of the spray impact region (location (4,4)) is much smaller than that measured in the film flow region (location (2,2)). At location (4,4), there was no change in the film thickness, within the measurement uncertainty, due to the addition of heat. This agrees with the results found in an earlier study that the heat removal mechanism underneath the spray is dominated by single-phase behavior [12]. Thus, since no evaporation of the liquid is expected for this applied heat flux, no change in film thickness is expected.

At location (2,2), the radius measured with applied heat flux is much smaller than the radius without heat (no mean film thickness could be calculated). However, visualization of the film flow outside of the spray suggests that the film is not thinner. Upon further investigation, when the images acquired where stepped through in order, it was discovered that the film could be seen "lifting off" of the surface, as shown in Fig. 9. The change in the ring radius, then, is not due to the disappearance of the film, but rather to the change of the index of refraction of the fluid on the surface of the die. It is no longer liquid FC-72; it is vapor FC-72. The index of refraction is lower than the liquid but higher than air, so the ring radii are slightly larger than the dry runs, when the flow was zero and there was air in the spray cap. This is evidence that the film is multiphase at location (2,2), and that the occurrence of dry vapor patches moving past is much more frequent than liquid.

Visualization of the liquid film beneath and around the sprays indicates that the film contains a significant gas fraction even under adiabatic conditions. However, the entrained bubbles in the adiabatic case never stick to the surface and cause dryout, and the fraction of liquid is high enough that, on average, a stable film thickness can be measured. The current results indicating frequent dryout in the film outside of the spray impact region agree quite well with the images presented by Horacek et al. [13]. Using a novel total internal reflection imaging technique, they were able to clearly image locations of dryout on a transparent heater. Significant dryout occurred in

Table 1
Measured radii and corresponding film thicknesses for the single-nozzle array, with and without an applied heat flux designs

Location	Flow rate [mL/s]	Power [W/cm^2]	Radius [pixels]	Film thickness [μm]
44	0	0	91.2	0
44	0.863	0	96.09	18.29
44	0.863	15	96.12	18.41
22	0	0	92.59	0
22	0.863	0	112.92	75.54
22	0.863	15	92.95	No film

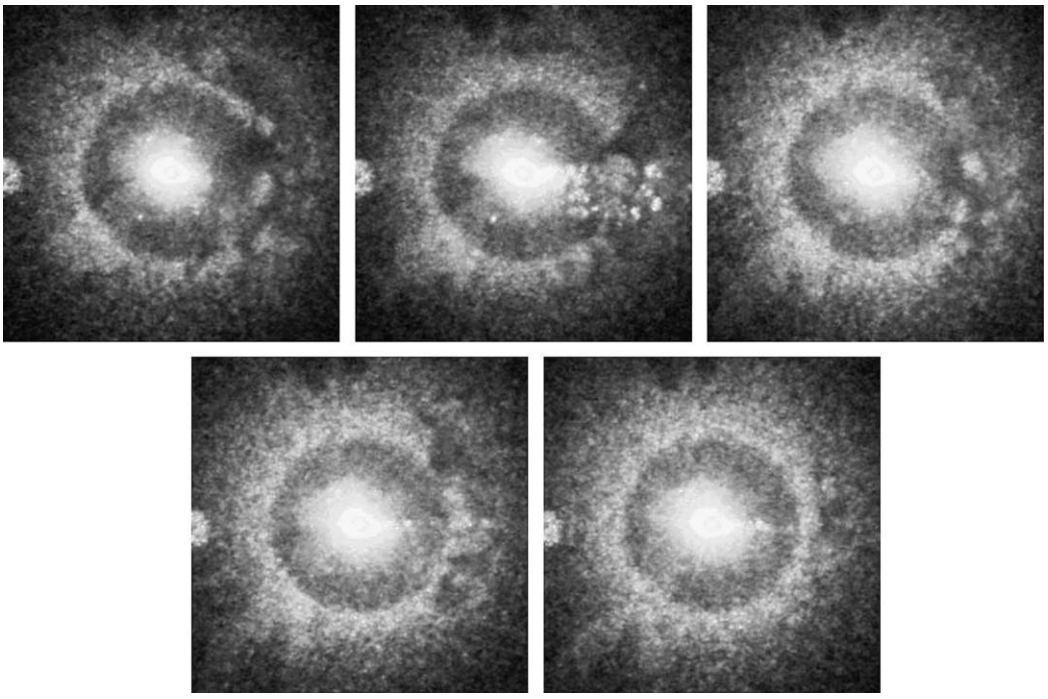

Fig. 9. Sequence of images showing the film "lifting off" at location (2,2) when power was applied. The images progress from left to right, top to bottom. The ring is seen on the right side of the first several images before it disappears. The images are 0.2 s apart.

their study at applied heat fluxes that were much lower than CHF.

5. Summary

A detailed study of the thin liquid film that forms due to single- and four-nozzle sprays has been presented. Local mean film thickness measurements were obtained using a non-intrusive optical film thickness measurement technique adapted for the spray system geometry. Important conclusions from this study include:

- The optical film thickness technique allows for detailed local film thickness distribution data to be obtained, even for the complex behaviors beneath interacting sprays. The mean film thickness measurements agree well with the qualitative imaging of the liquid film, except under the conditions where large vapor patches were present.
- Although the liquid film thickness generally correlated with previously measured heat transfer performance, these measurements do not provide direct evidence that the local film thickness is directly related to local heat transfer coefficients. The film thickness is a complicated function of the local velocity, the amount of entrained vapor and the interaction the film may have with flow from neighboring nozzles. All of these factors play a role in local heat flux removal.
- The film thickness in the spray impact region did not change measurably with applied heat flux. However, away from the spray impact, applied heat flux caused the growth of vapor patches to the point where extended periods of dryout were observed, in agreement with the work of Horacek et al. The surface would re-wet, however, so CHF did not occur.

Acknowledgements

The authors gratefully acknowledge the financial support of the University of Wisconsin Office of University–Industry Relations, Chester E. & Flora Jane LeRoy, and Cray, Inc. Contributions of spray analysis from Parker Hannifin Corp. are also appreciated.

References

[1] G. Pautsch, An overview on the system packaging of the CRAY SV2 supercomputer, in: Proceedings of IPACK'01, The Pacific Rim/ASME International Electronic Packaging Technical Conference and Exhibition, ASME, 2001, pp. 617–624.
[2] J. Yang, L.C. Chow, M.R. Pais, A. Ito, Liquid film thickness and topography determination using Fresnel diffraction and holography, Exp. Heat Transfer 5 (4) (1992) 239–252.
[3] D.E. Tilton, Spray cooling, Ph.D. thesis, University of Kentucky, Lexington, Kentucky, December 1989.
[4] W.S. Mathews, C.F. Lee, J.E. Peters, Experimental investigations of spray/wall impingement, Atomization Sprays 13 (2&3) (2003) 223–242.
[5] J. Li, Spray evaporative cooling in high heat flux electronics, Master's thesis, University of Minnesota, August 2000.
[6] T.A. Shedd, T.A. Newell, Automated optical liquid film thickness measurement method, Rev. Sci. Instrum. 69 (12) (1998) 4205–4213.
[7] A.G. Pautsch, Heat transfer and film thickness characteristics of spray cooling with phase change, Master's thesis, University of Wisconsin-Madison, Madison, Wisconsin, 2004.

[8] D.J. Rodíguez, T.A. Shedd, Cross-sectional imaging of the liquid film in horizontal two-phase annular flow, in: 2004 ASME Heat Transfer/Fluids Engineering Summer Conference, Charlotte, NC, 2004, paper 56445.
[9] The MathWorks, Inc., Matlab version 7.0.1, www.mathworks.com, 2005.
[10] T.A. Shedd, T.A. Newell, Characteristics of the liquid film and pressure drop in horizontal, annular, two-phase flow through round, square and triangular tubes, J. Fluids Eng. 126 (5) (2004) 807–817.
[11] A.G. Pautsch, T.A. Shedd, Spray impingement cooling with single- and multiple-nozzle arrays Part I: Heat transfer data using FC-72, Int. J. Heat Mass Transfer 48 (2005) 3167–3175.
[12] T.A. Shedd, A.G. Pautsch, Spray impingement cooling with single- and multiple-nozzle arrays. Part II: Visualization and empirical models, Int. J. Heat Mass Transfer 48 (2005) 3176–3184.
[13] B. Horacek, K.T. Kiger, J. Kim, Single nozzle spray cooling heat transfer mechanisms, Int. J. Heat Mass Transfer 48 (2005) 1425–1438.